Exergonic Intramolecular Singlet Fission of an Adamantane-Linked Tetracene Dyad via Twin Quintet Multiexcitons

Matsui, Yasunori ; Kawaoka, Shuhei ; Nagashima, Hiroki ; Nakagawa, Tatsuo ; Okamura, Naoki ; Ogaki, Takuya ; Ohta, Eisuke ; Akimoto, Seij…

(Citation)
The Journal of Physical Chemistry C,123(31):18813-18823

(Issue Date)
2019-07-08

(Resource Type)
journal article

(Version)
Accepted Manuscript

(URL)
https://hdl.handle.net/20.500.14094/90008039

Exergonic Intramolecular Singlet Fission of an Adamantane-linked Tetracene Dyad via Twin Quintet Multiexciton

Yasunori Matsui,[1,2] Shuhei Kawaoka,[1] Hiroki Nagashima,[3] Tatsuo Nakagawa,[4] Naoki Okamura,[1] Takuya Ogaki,[1] Eisuke Ohta,[1,2] Seiji Akimoto,[5] Shigeyuki Yagi,[1,2] Yasuhiro Kobori[3,5,*], and Hiroshi Ikeda[1,2,*]

[1]Department of Applied Chemistry, Graduate School of Engineering, Osaka Prefecture University, 1-1 Gakuen-cho, Nakaku, Sakai, Osaka 599-8531, Japan

[2]The Research Institute for Molecular Electronic Devices (RIMED), Osaka Prefecture University, 1-1 Gakuen-cho, Nakaku, Sakai, Osaka 599-8531, Japan

[3]Molecular Photoscience Research Center, Kobe University, 1-1 Rokkodai-cho, Nada-ku, Kobe, Hyogo 657-8501, Japan

[4]UNISOKU Co., Ltd. 2-4-3 Kasugano, Hirakata, Osaka 573-0131, Japan

[5]Graduate School of Science, Kobe University, 1-1 Rokkodai-cho, Nada-ku, Kobe, Hyogo 657-8501, Japan

KEYWORDS : Singlet Fission, Time-resolved EPR, Quintet State, Transient Absorption Spectroscopy

ABSTRACT: An adamantane-linked tetracene dyad (Tc–Ad–Tc) undergoes exergonic intramolecular singlet fission (SF), producing long-lived (τ = 175 μs) and high-energy (2 × 1.03 eV) multiexciton. Time-resolved absorption, fluorescence decay, and electron paramagnetic resonance (EPR) spectroscopic analysis revealed that the long-lived triplet species is generated in this system via correlated triplet pair having singlet and quintet characteristics. Time-resolved EPR analysis revealed formation of syn- and anti-conformers in the quintet, i.e. $^5(^3$Tc–Ad–^{3}Tc)*. The quintet generation requires small conformational motion to induce singlet-quintet spin relaxation. The presence of aliphatic linkages, like the rigid adamantane group, may enable effective conservation of intrinsic high S_1 and T_1 levels of the original monomers, moderate bridge-mediated σ–π interaction leading to exergonic intramolecular SF involving ^{1}Tc*–Ad–Tc → $^1(^3$Tc–Ad–^{3}Tc)*, and prevention of undesirable triplet–triplet annihilation, finally result in long-lived and high-energy multiexciton.

INTRODUCTION

The Singlet fission (SF) is a photophysical process in which interaction between one singlet-excited state (S_1) and ground state (S_0) species generates two triplet-excited species (T_1 + T_1).[1–3] Efficient SF requires that the energy level of the lowest excited singlet state (E_S) be larger than twice that of the excited triplet state ($2E_T$). Importantly, SF enables the maximum yield of triplet excitons to be 200% different from simple intersystem crossing (ISC) and, thus, it could be employed to improve the efficiencies of organic photovoltaics,[4,5] organic light-emitting diodes,[6] photodynamic therapies[7,8] and other applications.

SF requires strong interaction between neighboring molecules in the S_1 and S_0 states, thus typically occurs in the solid or aggregated states.[9–12] Typical SF description is displayed in eq 1,

$$S_1 + S_0 \rightarrow {}^1(TT) \rightarrow {}^5(TT) \rightarrow T_1 + T_1 \quad (1)$$

where S_1 and S_0 form two independent T_1, via the correlated triplet pairs[13] ^{1}(TT) and ^{5}(TT), having respective singlet and quintet multiplicities, that serves as key precursors of the independent T_1 molecules.

Construction of dyad of two π-systems using linker is a promising strategy to control interaction between them providing highly-efficient SF systems. Several studies have shown that intramolecular SF occurs in dyads of π-systems that contain linkers composed of conjugated[14–21] and/or nonconjugated[22–28] groups. Highly efficient intramolecular SF is reported using pentacene derivatives, owing to the presence of relatively large energy gaps between E_S (≈ 1.9 eV) and $2E_T$ (≈ 1.6 eV).[29] On the other hand, efficient intramolecular SF of tetracene derivatives are rarely known[30,31] because the energy gap is smaller ($E_S \approx 2E_T \approx$ 2.4 eV). The use of conjugated linkages often results in a decrease the energies of S_1 and T_1, which prevents exergonic SF. Also, achievement of high E_T level is important subject for practical use of SF, as a driving force of photoenergy conversion systems (1.1 eV for Si solar cell, 0.97 eV for $^1O_2$ generation). Nonconjugated linkages including sp^3-hybridized atoms are effective for maintaining the intrinsic high energies of S_1 and T_1 and enabling moderate interactions needed to trigger intramolecular SF. The sp^3-hybridized atoms also enable three-dimensional control of

interaction between two π-conjugated systems. Additionally, nonconjugated linkages can potentially prevent undesirable triplet–triplet annihilation (TTA), which is the reverse of SF. Thus, the use of nonconjugated linkages can enable formation of long-lived and high-energy excitons needed for practical applications of intramolecular SF.

In the investigation described below, we explored the SF behavior of two types of dyads, which contain tetracene moieties linked by an adamantane (Ad) moiety (Fig. 1). One dyad, Tc–Ad–Tc, possesses 5,12-bis((triisopropylsilyl)ethynyl)tetracene (Tc) moieties that are bonded to the 1- and 3-positions of Ad and the other, PTc–Ad–PTc, has phenyl-tetracene (PTc) moieties also at 1- and 3-positions of Ad. The pathway for SF in these dyads, exemplified by Tc–Ad–Tc, is shown in eq 2.

$$^1\text{Tc}^*\text{–Ad–Tc} \rightarrow {}^1(^3\text{Tc–Ad–}^3\text{Tc})^* \rightarrow {}^5(^3\text{Tc–Ad–}^3\text{Tc})^* \rightarrow {}^3\text{Tc}^*\text{–Ad–}^3\text{Tc}^* \quad (2)$$

Time-resolved absorption and EPR studies were carried out to characterize the intramolecular SF behavior of these dyads. The results show, that long-lived (τ = 175 μs) and high-energy (2 × 1.03 eV) triplet excitons are formed in Tc–Ad–Tc, which demonstrates the occurrence of exergonic intramolecular SF.

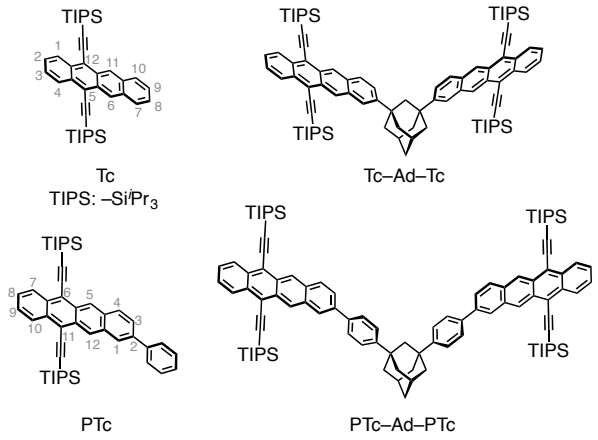

Fig. 1. Structures of Tc–Ad–Tc and PTc–Ad–PTc and the corresponding monomers. TIPS = triisopropylsilyl.

Experimental Section

General. Melting points (Mp) were obtained with a Yanaco MP-500 apparatus or differential scanning calorimetry (DSC) on Rigaku Thermo plus EVO II/DSC8230. ^{1}H and ^{13}C NMR spectra were recorded at 400 and 100 MHz, respectively, on a JEOL ECS400 spectrometer. Chemical shifts (δ) were reported in ppm using the signal of tetramethylsilane as an internal standard. IR spectra were recorded on a JASCO FT/IR 4100 spectrometer using attenuated total reflection (ATR) method. Atmospheric solid analysis probe (ASAP) mass measurements were carried out with a Shimadzu LCMS-2020 and LabSolutions LCMS software. Elemental analyses were carried out at the Research and Analytical Center at Kanazawa University.

Preparation of Substrates. Dyads Tc–Ad–Tc and PTc–Ad–PTc were synthesized according to Scheme 1. The structurally-related monomers Tc[32] and PTc[12] were also synthesized according to the literature.

Scheme 1. Synthetic Routes for Tc–Ad–Tc and PTc–Ad–PTc

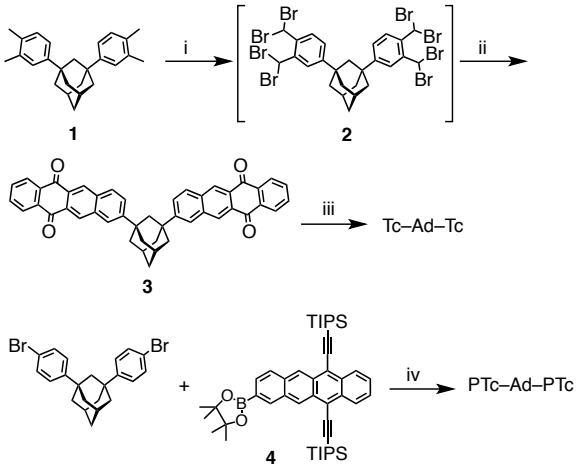

(i) NBS, BPO, CCl_4; (ii) 1,4-Naphthoquinone, KI, DMF; (iii) (Triisopropylsilyl)ethyne, *n*-BuLi, followed by sat. $SnCl_2$•$2H_2O$ in 10% aq. HCl; (iv) K_2CO_3, Pd(dppf)Cl_2, THF/H_2O.

1,3-Bis(3,4-bis(dibromomethyl)phenyl)adamantane (2). A CCl_4 (30 mL) solution of 1,3-bis(3,4-dimethylphenyl)adamantane (**1**, 3.44 g, 10 mmol), *N*-bromosuccinimide (NBS, 7.55 g, 42 mmol), and benzoyl peroxide (BPO, 246 mg) were stirred at reflux (85 °C) under an argon atmosphere for 5 h in the dark. Additional NBS (7.26 g, 41 mmol) and BPO (246 mg) were added to the mixture, which was then stirred at reflux for 15 h in the dark. The mixture was cooled to room temperature and filtered. The precipitate was washed with CH_2Cl_2. The combined filtrates were washed with water (30 mL × 2) and sat. aq. $NaHSO_3$ (30 mL), dried over Na_2SO_4, and then concentrated under reduced pressure to give crude **2** (5.84 g), which was used in the next reaction.

1,3-Bis(tetracen-5,12-dion-8-yl)adamantane (3). A dry *N*,*N*-dimethylformamide (DMF, 50 mL) solution of **2** (5.84 g), 1,4-naphthoquinone (1.87 g, 12 mmol) and KI (7.97 g, 48 mmol) was stirred at 110 °C under argon atmosphere for 24 h. The mixture was cooled to room temperature and poured into 300 mL of CH_3OH. The precipitate was collected by filtration, washed with CH_3OH and dissolved in $CHCl_3$. The $CHCl_3$ solution was washed with water (100 mL × 2), sat. aq. $NaHSO_3$ (100 mL) and brine (100 mL), dried over Na_2SO_4, and then concentrated under reduced pressure. Re-precipitation of the $CHCl_3$ solution into CH_3OH of the solid gave **3** (2.17 g, 3.35 mmol, y. 61% for two steps) as brown powder. Mp = 294 °C (DSC); ^{1}H NMR (400 MHz, $CDCl_3$) δ_{ppm} 1.93 (br, 2H), 2.13–2.19 (m, 8H), 2.28 (s, 2H), 2.50 (br, 2H), 7.81–7.88 (m, 6H), 8.05 (s, 2H), 8.08 (d, J = 8.8 Hz, 2H), 8.38–8.41 (m, 4H), 8.83 (s, 2H), 8.85 (s, 2H); ^{13}C NMR (100 MHz, $CDCl_3$) δ_{ppm} 29.5 (2C), 35.8, 38.1 (2C), 42.0 (4C), 48.4, 125.5 (2C), 127.6 (2C + 2C), 128.0 (2C), 129.3 (2C), 129.6 (2C), 129.8 (2C), 130.0 (2C), 130.2 (2C), 133.9 (2C), 134.2 (2C + 2C), 134.69 (2C),

134.72 (2C), 135.6 (2C), 152.0 (2C), 183.2 (2C + 2C); IR (ATR) ν/ cm^{-1} 2902, 1675, 1279, 965, 711; LR-mass (FAB, 3-nitrobenzyl alcohol (NBA)) m/z = 648 (M^+).

1,3-Bis(5,12-bis((triisopropylsilyl)ethynyl)tetracen-8-yl)adamantane (Tc–Ad–Tc). To a solution of (triisopropylsilyl)ethyne (2.7 mL, 12 mmol) in dry tetrahydrofuran (THF, 15 mL) at –78 °C under argon was added *n*-BuLi in hexane (1.55 M, 6.5 mL, 10 mmol). The resulting solution was stirred for 1 h and warmed to –20 °C before adding a THF (10 mL) solution of **3** (1.30 g, 2 mmol). The solution was then allowed to warm to room temperature before adding an excess of sat. $SnCl_2$•H_2O in 10% aq. HCl. After stirring for 2 h at room temperature, the mixture was extracted with CH_2Cl_2 (30 mL × 3). The CH_2Cl_2 extracts were dried over Na_2SO_4 and concentrated under reduced pressure. The residue was subjected to silica-gel column chromatography (*n*-hexane/CH_2Cl_2 = 4/1), followed by recrystallization from 2-butanone to give Tc–Ad–Tc (376 mg, 0.29 mmol, y. 14%) as red powder. Mp ≈ 260 °C (decomp., DSC); ^{1}H NMR (400 MHz, $CDCl_3$) δ_{ppm} 1.29–1.38 (m, 84H), 1.95 (br, 2H), 2.19 (m, 8H), 2.30 (s, 2H), 2.52 (br, 2H), 7.52–7.54 (m, 4H), 7.66 (d, J = 9.2 Hz, 2H), 7.89 (s, 2H), 8.00 (d, J = 9.2 Hz, 2H), 8.60–8.63 (m, 4H), 9.26 (s, 2H), 9.29 (s, 2H); ^{13}C NMR (100 MHz, $CDCl_3$) δ_{ppm} 11.75 (6C), 11.77 (6C), 19.1 (12C + 12C), 29.7 (2C), 36.2, 37.7 (2C), 41.7 (4C), 48.0, 104.2 (2C + 2C), 105.77 (2C), 105.81 (2C), 118.5 (2C), 118.7 (2C), 122.8 (2C), 125.2 (2C), 125.8 (2C), 126.2 (2C), 126.6 (2C), 126.7 (2C), 127.5 (2C + 2C), 128.5 (2C), 130.4 (2C), 130.7 (2C), 131.3 (2C), 132.5 (2C + 2C), 132.7 (2C), 147.9 (2C); LR-mass (FAB, NBA) m/z = 1310 ([M+H]$^+$). Anal. Calcd for $C_{90}H_{116}Si_4$: C, 82.50; H, 8.92; Si, 8.57. Found: C, 82.14; H, 9.02; N, 0.13.

1,3-Bis(4-(5,12-bis((triisopropylsilyl)ethynyl)tetracen-8-yl)phenyl)adamantane (PTc–Ad–PTc). A THF/water (50 mL/5 mL) solution of 2-(4,4,5,5-tetramethyl-1,3,2-dioxaborolan-2-yl)-6,11-bis((triisopropylsilyl)ethynyl)tetracene[32] (**4**, 1.57 g, 2.2 mmol), 1,3-bis(4-bromophenyl)adamantane (450 mg, 1.0 mmol), (1,1'-bis(diphenylphosphino)ferrocene)palladium(II) dichloride (81 mg, 0.11 mmol) and K_2CO_3 (2.43 g, 18 mmol) was stirred at reflux (75 °C) under argon atmosphere for 24 h in the dark. After filtration through Celite pad, the mixture was extracted with $CHCl_3$ (80 mL × 3). The $CHCl_3$ extracts were dried over Na_2SO_4 and then concentrated under reduced pressure to give a residue that was subjected to silica-gel column chromatography (*n*-hexane/EtOAc = 20/1), followed by recrystallization from *n*-hexane to give PTc–Ad–PTc (1.10 g, 0.75 mmol, y. 75%) as red powder. Mp ≈ 250 °C (decomp., DSC); ^{1}H NMR (400 MHz, $CDCl_3$) δ_{ppm} 1.31–1.39 (m, 84H), 1.88 (br, 2H), 2.09 (br, 8H), 2.22 (s, 2H), 2.42 (br, 2H), 7.53–7.56 (m, 4H), 7.61 (AA'BB', J = 8.4 Hz, 4H), 7.77 (d, J = 9.2 Hz, 2H), 7.80 (AA'BB', J = 8.4 Hz, 4H), 8.09 (d, J = 9.2 Hz, 2H), 8.19 (s, 2H), 8.63 (dd, J = 6.8, 2.7 Hz, 4H), 9.32 (s, 2H), 9.34 (s, 2H); ^{13}C NMR (100 MHz, $CDCl_3$) δ_{ppm} 11.8 (6C + 6C), 19.1 (12C + 12C), 29.8 (2C), 36.1, 37.4 (2C), 42.5 (4C), 49.2, 104.1 (2C + 2C), 105.97 (2C), 106.05 (2C), 118.6 (2C), 118.8 (2C), 125.7 (2C), 125.8 (4C), 126.2 (2C), 126.6 (2C + 2C), 126.8 (2C), 126.9 (2C), 127.3 (4C), 127.6 (2C + 2C), 129.3 (2C), 130.6 (2C), 130.8 (2C), 131.5 (2C), 132.6 (2C), 132.7 (2C), 132.9 (2C), 138.3 (2C), 138.5 (2C), 150.4 (2C); LR-mass (FAB, NBA) m/z = 1462 ([M+H]$^+$); Anal. Calcd for $C_{102}H_{124}Si_4$: C, 83.77; H, 8.55. Si, 7.68. Found: C, 83.50; H, 8.59.

Spectroscopic Measurements

UV–Vis absorption and photoluminescence spectra were recorded on JASCO V-570 and FP-8500 spectrophotometers, respectively. Absolute fluorescence quantum yields were determined by utilizing the integrating sphere method with a Hamamatsu Photonics C9920-02. Fluorescence lifetime were determined by using a HORIBA Jobin Yvon FluoroCube time-correlated single photon counting photometer and analyzed using Igor Pro software. Phosphorescence spectra were measured at 77 K on a HORIBA Jobin Yvon Fluorolog-3 spectrophotometer with a VT CBL-LR/RM12 Dewar adopter and a DSS-IGA020L near-infrared detector with visible cutoff filter.

Time-resolved Absorption Spectroscopic Measurements. Subnanosecond transient absorption studies were carried out using a UNISOKU picoTAS spectrophotometer, which is based on a recently-developed randomly-interleaved pulse train (RIPT) method.[33] The pump source is a picosecond YAG laser (355 nm, EKSPLA PL-2210A, 1 kHz, fwhm = 25 ps) equipped with an optical parametric generator (EKSPLA PG403, 410–700 nm, 50 μJ pulse^{-1} @500 nm), and the probe source is a supercontinuum radiation source (410–2000 nm, LEUKOS SMHP-20.2, 20 MHz, fwhm = 50–100 ps). The reliability has been demonstrated by its use in many studies of photoinduced electron transfer and artificial photosynthetic systems.[34–37] Time-resolution of the system was estimated to be ≈ 80 ps. Measurements were conducted by using a sample solution with an optical density (*OD*) = 0.6 at excitation wavelength in a vessel of 2 mm thickness under argon flow conditions. Spectroscopic data were analyzed by using Glotaran software.[38] Nano–micro–millisecond transient absorption was measured on a UNISOKU TSP-1000 setup with YAG laser (355 nm, Spectra Physics Quanta-Ray GC-100, 10 Hz, fwhm = 8 ns, 15 mJ pulse^{-1}) excitation and Xe arc monitoring lamp (150 W).

Time-resolved EPR Measurements. Continuous wave time-resolved EPR measurements were performed using a Bruker EMXplus spectrometer. The detailed experimental settings have been described previously.[39] Photoexcitations were performed by using the second harmonics of a Nd:YAG laser (532 nm, Continuum Minilite II, 10 Hz, fwhm = 5 ns). A light depolarizer was placed between the laser output and the optical window of the EPR cavity.[39]

Theoretical Calculations. Density functional theory (DFT) calculations were carried out using Gaussian 09W program[40] using B3LYP functional and 6-31G(d) or 6-31G(d,p) basis set. To reduce the computational costs, TIPS groups were replaced by trimethylsilyl (TMS) groups, noted as Tc' for the ground states. Optimized geometries of the quintet states were obtained both for Tc–Ad–Tc and Tc'–Ad–Tc'. It was confirmed that the conformations of the aromatic-rings were unaffected by the Tc'

replacement. Geometries and orbitals were plotted by using an Avogadro[41] or Gaussview[42] program.

RESULTS AND DISCUSSION

Theoretical Study. Theoretical studies were carried out on the Ad-linked dyads, Tc'–Ad–Tc' and PTc'–Ad–PTc', using models in which TIPS containing Tc moieties are replaced by the more simple TMS containing Tc' analogs. Geometries of the dyads and the corresponding individual components Tc' and PTc' were optimized by using DFT calculations at the B3LYP/6-31G(d) level of theory (Fig. 2). At least two local energy minimum geometries, corresponding to anti- and syn-conformers, were obtained for Tc'–Ad–Tc'. The anti-conformation, having a lower energy, is displayed in Fig. 2a while the syn-conformation (+1.6 kcal mol^{-1} in S_0, +0.31 kcal mol^{-1} using CAM-B3LYP) will be discussed later. Distances between C2 atoms of Tc'–Ad–Tc' and PTc'–Ad–PTc' were found to be 5.1 and 12.2 Å, respectively. In the minimum energy anti-conformer of Tc'–Ad–Tc', the planes of one of the tetracene moieties is tilted by ≈ 90° with respect to the other, but it is nearly freely rotatable on the NMR timescale at room temperature. Recently, Shigeta *et al.* reported that the distance between two π-conjugated systems needs to be shorter than 10 Å in order for efficient TTA to take place.[43] Also, Liang *et al.* showed that SF is not enhanced in system that have co-facial orientations of the two π-systems but it is in those that have these moieties in *J*-aggregate orientation.[44] The results of our calculations show that only Tc'–Ad–Tc' and not PTc'–Ad–PTc' has a geometry that satisfies these conditions. Thus, Tc'–Ad–Tc' is expected to display efficient intramolecular SF.

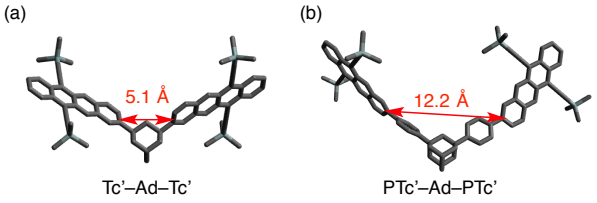

Fig. 2. Optimized geometries of (a) Tc'–Ad–Tc' in anti-type conformation and (b) PTc'–Ad–PTc' in the S_0 states with the distances between the C2 atoms in tetracene moieties (B3LYP/6-31G(d)).

Determination of Excited Energy Levels. UV–Vis absorption, fluorescence, and phosphorescence spectra of Tc and Tc–Ad–Tc in methylcyclohexane (MCH) were measured (Fig. 3a). The results show that Tc and Tc–Ad–Tc have π,π* absorption maxima at 531 and 532 nm, respectively, and that the molar absorption coefficient (ε) of Tc–Ad–Tc is almost twice that of Tc (3.6×10^4 $M^{-1}cm^{-1}$). Similarly, Tc and Tc–Ad–Tc display respective fluorescence maxima at 539 and 545 nm. The emission maximum of Tc–Ad–Tc is slightly red-shifted and broadened as compared with that of Tc, indicating that weak exciton coupling takes place between two Tc moieties in the dyad. That the shift is small suggests that Tc–Ad–Tc has an E_S that is as high as that of Tc, a likely consequence of the fact that the angle between the transition dipole moments in the Tc moieties is sufficient to suppress the Davydov splitting in both the anti- and syn-conformations. The fluorescence quantum yield (Φ_{FL}) of Tc–Ad–Tc was determined to be 0.26, a value which is remarkably smaller than that of Tc (0.72).[45] Phosphorescence maxima of both Tc and Tc–Ad–Tc in frozen (77 K) MCH solutions were observed at 1220 nm. Thus, respective E_S and E_T for Tc–Ad–Tc are 2.28 and ≈ 1.02 eV (Table 1). These results suggest that SF of Tc–Ad–Tc ($E_S > 2E_T$) finally providing ^{3}Tc*–Ad–^{3}Tc* is exergonic. Note that E_T of Tc is lower than the value reported in literature (≈ 1.2 eV),[45] suggesting that stabilization of T_1 is caused by the presence of silylethynyl groups, a proposal that is supported by the results of DFT calculations.[46]

PTc–Ad–PTc displays absorption, fluorescence, and phosphorescence maxima at 541, 547, and 1200 nm, respectively (Fig. 3b, Table 1). The magnitude of the shift in fluorescence maxima between PTc–Ad–PTc and PTc are slightly smaller than those between Tc–Ad–Tc and Tc pair. E_S and E_T of PTc–Ad–PTc were determined to be 2.27 and ≈ 1.03 eV, respectively, values that satisfy conditions of $E_S > 2E_T$ needed for exergonic SF. The respective Φ_{FL} values of PTc and PTc–Ad–PTc were determined to be 0.33 and 0.30. The results suggest that the Ad linkage in the dyads prevents unnecessary stabilizations of E_S and E_T leading to effective conservation of intrinsic E_S and E_T of the π-conjugated components.

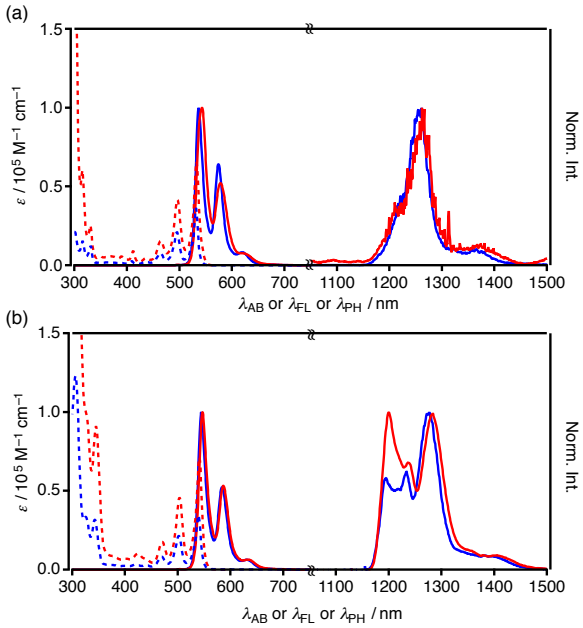

Fig. 3. UV–Vis absorption (dotted), fluorescence, and phosphorescence (solid) spectra of (a) Tc (blue) and Tc–Ad–Tc (red) and (b) PTc (blue) and PTc–Ad–PTc (red) in MCH. Phosphorescence spectra were measured using MCH matrices at 77 K.

Fluorescence Decay Profiles. Fluorescence decay profiles for Tc and Tc–Ad–Tc in degassed MCH at room temperature were

Table 1. Photophysical Properties of Tc, Tc–Ad–Tc, PTc, and PTc–Ad–PTc Measured in MCH at Room Temperature

Compound[a]	λ_{AB} / nm	ε / 10^4 $M^{-1}cm^{-1}$	λ_{FL} / nm	λ_{PH}[b] / nm	Φ_{FL}	τ_{FL} / ns (ratio / %)	k_{FL} / 10^7 s^{-1}	k_{NR} / 10^7 s^{-1}	k_{ISC} / 10^7 s^{-1}	E_S / eV	E_T / eV
Tc	531	3.6	537	1220	0.72	11.5 (100)	6.3	0.7	1.7	2.31	1.02
Tc–Ad–Tc	532	6.5	543	1220	0.26	4.0 (91.3) 10.1 (8.4) 435.4 (0.3)	(6.3)[c]	(0.7)[c]	(1.7)[c]	2.28	1.02
PTc	539	3.5	545	1195	0.33	6.9 (100)	5.4	1.5	7.6	2.28	1.04
PTc–Ad–PTc	541	7.1	547	1200	0.30	6.8 (100)	5.0	1.4	8.3	2.27	1.03

[a][Tc] = [PTc] = 20 μM, [Tc–Ad–Tc] = [PTc–Ad–PTc] =10 μM. [b]At 77 K. [c]Estimated from the values of the corresponding monomers.

measured by using the time-correlated single photon-counting method. The fluorescence decay profile of Tc against time (t), displayed in Fig. 4a, easily fit by using a single exponential function, shows that it has a lifetime (τ_{FL}) of 11.5 ns. On the other hand, fitting of fluorescence decay curve of Tc–Ad–Tc (Fig. 4c, red) requires the use of the triple exponential functions, given in eq 3.

$$I(t) = A_1\exp(-t/\tau_{FL1}) + A_2\exp(-t/\tau_{FL2}) + A_3\exp(-t/\tau_{FL3}) \quad (3)$$

This treatment gives τ_{FL} values of 4.0 (91.3%, τ_{FL1}), 10.1 (8.4%, τ_{FL2}), and 435.4 ns (0.3%, τ_{FL3}). The presence of the fastest components suggests the occurrence of SF for ^{1}Tc*–Ad–Tc. Note that the τ_{FL3} component was not detected when an aerated condition was used (Fig. 4c, blue), suggesting that it is associated with a triplet species that is readily quenched by molecular oxygen. Owing to concentration considerations, *inter*molecular TTA of two free ^{3}Tc*–Ad–Tc would be negligible on this short timescale. Thus, ^{1}Tc*–Ad–Tc is regenerated by *intra*molecular TTA in ^{3}Tc*–Ad–^{3}Tc*.This delayed fluorescence behaviour of Tc–Ad–Tc is similar to the results of tetracene derivatives reported by Thompson and co-workers.[17] Although this TTA process of ^{3}Tc*–Ad–^{3}Tc* should be endergonic by 0.24 eV, reverse ISC[47–49] is widely known as an example where such an endergonic process occurs within 100 ns timescale. The energetic difference of 0.24 eV is reasonable, because a threshold whether reverse ISC occurs at room temperature is empirically estimated to be ≈ 0.3 eV.

Rate constants for fluorescence emission (k_{FL}), nonradiative deactivation (k_{NR}), and ISC (k_{ISC}) of Tc and PTc, obtained by using eqs 4 and 5, are listed in Table 1.

$$\Phi_{FL} = k_{FL}/(k_{FL} + k_{NR} + k_{ISC}) \quad (4)$$

$$k_{FL} + k_{NR} + k_{ISC} = k_S = 1/\tau_{FL} \quad (5)$$

The fluorescence decay profile of PTc–Ad–PTc (τ_{FL} = 6.8 ns, Fig. 4b) is almost the same as that of PTc (τ_{FL} = 6.9 ns, Fig. 4d), showing that PTc–Ad–PTc does not undergo remarkable intramolecular SF even though the relationship $E_S > 2E_T$ is satisfied. The absence of SF is likely a consequence of the relatively long distance (12.2 Å) between the two Tc moieties in PTc–Ad–PTc. Moreover, PTc–Ad–PTc and PTc have almost the same k_{FL} and k_{NR} values, supporting that k_{NR}, k_{FL}, and k_{ISC} for Tc–Ad–Tc can be estimated by using those of Tc. Note that no delayed fluorescence was observed for PTc and PTc–Ad–PTc (Fig. 4b,d), even if k_{ISC} of them are higher than that of Tc.

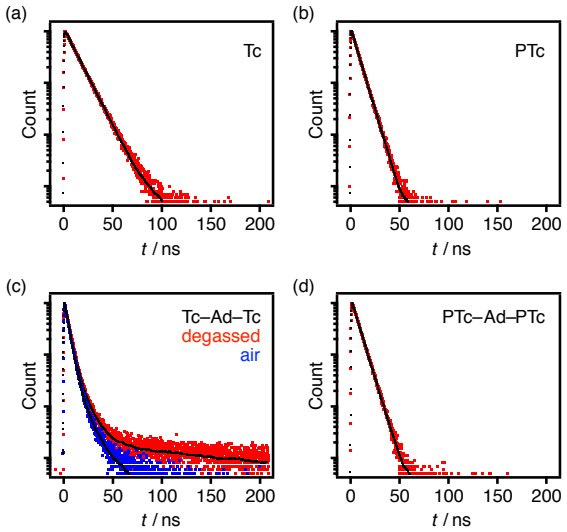

Fig. 4. Fluorescence decay profiles of (a) Tc, (b) PTc, (c) Tc–Ad–Tc, and (d) PTc–Ad–PTc in (red) degassed and (blue) aerated MCH detected at respective λ_{FL} maxima. Black curves are fitted lines. The values for τ_{FL} are listed in Table 1. [Tc] = [PTc] = 20 μM, [Tc–Ad–Tc] = [PTc–Ad–PTc] = 10 μM.

Time-resolved EPR Measurement. Time-resolved EPR measurements were made in order to identify the species generated by fluorescence quenching of ^{1}Tc*–Ad–Tc. The results show that photoexcitation of a frozen 2-methyltetrahydrofuran (MTHF) solution of Tc–Ad–Tc (50 μM) at 110 K leads to production of multiple EPR resonance lines centered around g = 2.002 (340 mT), which are displayed in black in Fig. 5a. Splitting of peaks between the largest emission/absorption (E/A) polarization intensities was 15 mT, which is similar to that of the quintet EPR signals as the strongly correlated multiexciton.[10] However, additional inner A/E polarized peak splitting is observed together with a broad A/E polarized larger splitting of ≈ 40 mT, suggesting the occurrence of multiple spin–spin interactions in the correlated triplet pairs. Moreover, contributions to the EPR line-shapes from non-correlated triplet species (^{3}Tc*–Ad–Tc and weakly coupled ^{3}Tc*–Ad–^{3}Tc*) are absent in the spectrum under frozen conditions. Thus, spin-orbit coupling-assisted ISC is negligible in this system.

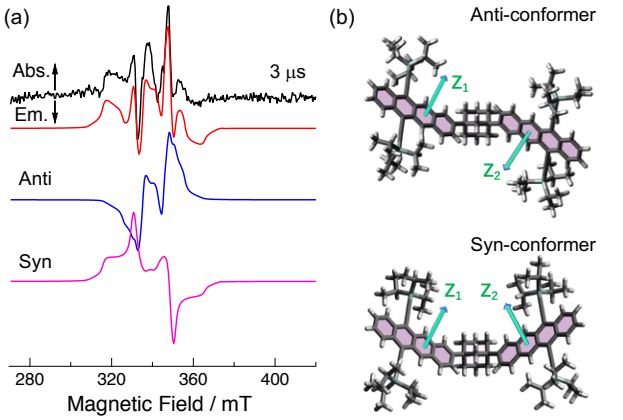

Fig. 5. (a) Time-resolved EPR spectra of Tc–Ad–Tc (5.0×10^{-5} M) in degassed MTHF at 110 K. Microwave frequency was 9.542 GHz and the delay time after the flash was 3 μs. Black and red lines are experimental and simulated spectra, respectively. Blue and purple lines are computed spectra corresponding to conformers with respective tilt angles of 89° and 56° between the two out-of-plane principal Z axes of the ZFS tensor of the individual tetracene moieties (respective upper and lower structures in (b)). Fitting parameters are given in Table S7 in the Supporting Information. (b) Geometries of the anti- and syn- conformers of $^5(^3$Tc–Ad–^{3}Tc)* calculated by using B3LYP/6-31G(d,p) with respective principal Z axes of $\boldsymbol{D}_1$ tensor. The Cartesian coordinates are given in Tables S8 and S9 in the Supporting Information.

In a previous effort, we observed SF-born quintet EPR signals arising from solute aggregates, prepared by freezing 10^{-4} M CH_2Cl_2 solutions of 6,13-bis((triisopropylsilyl)ethynyl)pentacene and PTc. This finding demonstrated that intermolecular SF produces the quintet pair ^{5}(TT) within the aggregates.[12] However, the absence of quintet EPR signals from a solution of Tc in frozen MTHF excludes the possibility that Tc aggregates form. Also, no aggregation-induced line broadening is present in the absorption spectrum of Tc–Ad–Tc in MTHF at 77 K (Fig. S2 in the Supporting Information). Thus, it is reasonable to conclude that the multiple-line EPR signals (Fig. 5a) are not caused by intermolecular SF in Tc–Ad–Tc.

Previous reports[10,12,50–53] described a simulation method for treating strongly correlated triplet pairs that involves diagonalizing the spin Hamiltonian from the nine basis spin functions from the quintet, triplet, and singlet TT pairs. By using this method, the spin Hamiltonian composed of the Zeeman interaction ($\boldsymbol{H}_{\mathrm{TTZ}}$), spin–spin dipolar coupling ($\boldsymbol{H}_{\mathrm{TTzfs}}$), and an exchange interaction ($\boldsymbol{H}_{\mathrm{TTee}} = 2J\mathbf{S}_1\mathbf{S}_2$, where $J$is exchange coupling constant) was diagonalized to obtain quintet sublevel eigenvalues for creation of a simulated EPR spectrum. In $\boldsymbol{H}_{\mathrm{TTzfs}} = h\mathbf{S}_1\boldsymbol{D}_1\mathbf{S}_1 + h\mathbf{S}_2\boldsymbol{D}_2\mathbf{S}_2$, h is the Planck constant, $\mathbf{S}_i$ is the i-th (i = 1, 2) triplet spin operator in the dimer, and $\boldsymbol{D}_i$ represents the zero-field splitting (ZFS) tensor of the individual triplet Tc. As a result, the matrix of the $\boldsymbol{H}_{\mathrm{TTzfs}}$ tensor is dependent on the orientation of the principal axes in the $\boldsymbol{D}_2$ tensor (X_2, Y_2, Z_2) with respect to the principal axes in $\boldsymbol{D}_1$ tensor (X_1, Y_1, Z_1). Therefore, the $\boldsymbol{D}_2$ orientation could affect the EPR pattern in the quintet. As was done in the previous study,[12] the geometries of the second Tc groups were generated by using relative Euler rotation angles with respect to the principal axes in $\boldsymbol{D}_1$. In order to assign the time-resolved EPR peaks, two different conformers were considered. When two different $\boldsymbol{D}_2$ tensors, whose principal Z_2 axes are tilted by 89° and 56° with respect to the Z_1 axes (Fig. 5b) of $\boldsymbol{D}_1$, are considered, two different time-resolved EPR spectra are produced (respective blue and purple lines in Fig. 5a). The sum of these spectra, indicated by a red line in Fig. 5a, well reproduces the experimental spectrum as the strongly coupled ^{3}Tc*–Ad–^{3}Tc*s. The spin polarization calculations and fitting parameters are given below and in Table S7 in the Supporting Information. This finding strongly supports the proposal that S_1 quenching takes place by the intramolecular SF.

The results of B3LYP/6-31G(d,p) level calculations on the geometries of the quintet multiexciton indicated the presence of two optimized conformers of $^5(^3$Tc–Ad–^{3}Tc)* that have similar total energies (ΔE = 0.13 kcal mol^{-1}). The tilt angles between the Z_2-axes of the tetracene moieties in the optimized conformers were observed to be 90° and 64° and correspond to the respective anti- and syn-conformers of $^5(^3$Tc–Ad–^{3}Tc)* (Fig. 5b). These angles are almost identical to the Euler angles used for the spectral simulations shown in Fig. 5a.

To examine the mechanism for quintet generation following SF, the time-profile of the transient EPR signal was obtained at 348 mT (Fig. S3 in the Supporting Information). The rises in the EPR signals were much slower (time constant = 0.9 μs) than the instrument response time, although SF needs to occur within the nanosecond regime shorter than the fluorescence lifetime (12 ns) of ^{1}Tc*. This observation suggests that the quintet states $^5(^3$Tc–Ad–^{3}Tc)* are populated by spin-relaxations of the long-lived $^1(^3$Tc–Ad–^{3}Tc)* (eq 2). Thus, the spin-relaxation would be accompanied by small conformational dynamics[54] in the anti- and syn-conformers (Fig. 5b) at 110 K in MTHF glass,[55,56] rather than by triplet exciton diffusion to create chemically induced dynamic election polarization[12] within the multiexciton in the aggregates. Because singlet–triplet (S–T_0) relaxation processes are reported to take place by modulations of J in radical pairs at cryogenic temperatures,[39,57] a fluctuation in J associated with the above conformation motions could promote singlet–quintet relaxation through $\boldsymbol{H}_{\mathrm{TTzfs}}$ in the present system, even though the energy difference between quintet and singlet states are dominated by intramolecular J.

In the simulation (Fig. 5a), the spin polarization patterns were well reproduced when quintet sublevel populations at m_S = –2, –1, 0, +1 and +2 were dependent of the magnetic-field direction in the multiexciton in accordance with the direction dependence of $\boldsymbol{H}_{\mathrm{TTzfs}}$.[12] The quintet sublevel populations were computed by eq 6

$$W_{m_s} = \frac{2}{\hbar^2} < \mathrm{Q}_{m_s}|\boldsymbol{H}_{\mathrm{TTzfs}}|\mathrm{S} >^2 \frac{2\tau_c}{1+\omega_{m_s}^2\tau_c^2} \qquad (6)$$

as the spin-lattice relaxation rate constants,[58] where Q_{m_s} and S represent $^5(^3$Tc–Ad–^{3}Tc)* and $^1(^3$Tc–Ad–^{3}Tc)*, respectively. The term ω_{m_s} denotes the singlet-quintet energy gaps in the multiexciton dominated by the Zeeman splitting and J (≈ –25 GHz). The value τ_C = 100 ps was assumed as the correlation time of the J-fluctuations. The fitting result strongly supports that the quintet generation is governed by probability finding $^1(^3$Tc–Ad–

^{3}Tc)* mixed though $\boldsymbol{H}_{TTzfs}$, in ^{5}(^{3}Tc–Ad–^{3}Tc)* in the presence of the field and J.

Transient Absorption Spectroscopic Analysis. Subnanosecond to microsecond transient absorption spectroscopic analysis was conducted on Tc–Ad–Tc and Tc using RIPT and CW probe methods. Photoexcitation of Tc at 531 nm in degassed MCH at room temperature produced an absorption profile in the <10-ns regime (Fig. S6 in the Supporting Information) that contains a positive absorption band at 425 nm assigned to ^{1}Tc*. If contributions of stimulated emission and absorption of ^{1}Tc* can be disregarded in the 495-nm bleaching band, $\Delta\varepsilon$ of ^{1}Tc* at 425 nm is estimated to be 1.32×10^5 $M^{-1}cm^{-1}$. A slight increase in the intensity of a long-lived band 505 nm band occurs after 10 ns, which is assigned to ^{3}Tc* that is generated by ISC, and decayed with single exponential manner with $\tau = 45$ μs (Fig. 6c, blue). If the 495-nm bleaching bands is exclusively attributed by ground-state absorption, $\Delta\varepsilon$ of ^{3}Tc* at 505 nm is estimated to be 4.71×10^4 $M^{-1}cm^{-1}$.[31,45] The results of multi-wavelength global analysis show that these profiles can be explained in terms of two components corresponding to decay of ^{1}Tc* and, rise and decay of ^{3}Tc*. Rate constants for decay of ^{1}Tc* and rise of ^{3}Tc* were determined to be 8.7×10^7 and 1.7×10^7 s^{-1}, respectively. The value of $\Phi_T = 0.19$ for Tc was determined by using these rate constants.

Photoexcitation of Tc–Ad–Tc using the same conditions also gave transient absorption profiles in the <10-ns regime that contain a decaying band at 420 nm, a rising then decaying band at 515 nm, and a negative band at 535 nm (Fig. 6a,b). Results of an earlier study with an adamantane-linked pentacene[23] suggest that the absorption spectra of ^{3}Tc*–Ad–Tc, ^{1or5}(^{3}Tc–Ad–^{3}Tc)* and ^{3}Tc*–Ad–^{3}Tc* should be nearly indistinguishable. If $\Delta\varepsilon$ for ^{1}Tc* and ^{3}Tc* moiety in Tc–Ad–Tc are identical to those in Tc, $\Phi_T = 0.92$ for Tc–Ad–Tc, at 15 ns after laser excitation. Decay of the 505-nm absorption band takes place in two steps ($\tau = 188$ ns and 175 μs (Fig. 6c, red)), which is typical for efficient SF systems. The faster component is shorter than the triplet lifetime of Tc (45 μs) due to the existence of TTA process. On the other hand, the slower process is sufficiently long to enable export of triplet excitons to outside of the system. Note that k_T for Tc–Ad–Tc (5.7×10^3 s^{-1}) is smaller than that of Tc (2.1×10^4 s^{-1}), which is typical for the dyad system,[15,30] probably due to delocalization of exciton.

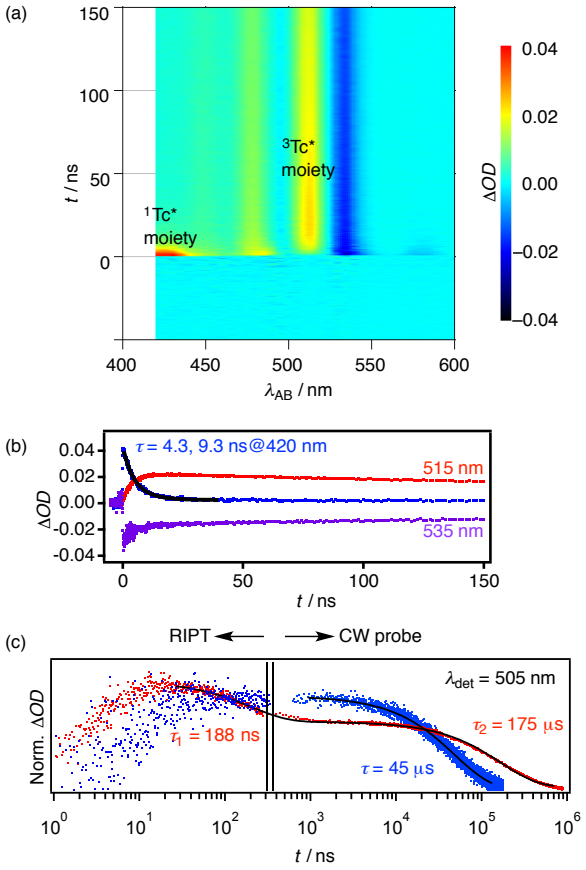

Fig. 6. 3D-Subnanosecond transient absorption spectra of (a) Tc–Ad–Tc in degassed MCH (40 μM). Positive and negative absorption are designated using the color profiles shown in the side bar. (b) Time-profiles observed at (red) 420, (blue) 515, and (purple) 535 nm with (black) fitted curve. (c) Nano-to-millisecond decay profiles for (red) Tc–Ad–Tc and (blue) Tc traced at 505 nm using RIPT and CW probe methods for the region shorter and longer than 200 ns, respectively. ΔOD values were normalized at 200 ns. Two-components of the decay profile possessing time constant of 188 ns and 175 μs for Tc–Ad–Tc.

Kinetic Analysis Based on Various Spectroscopic Measurements. A combined energy profile and kinetic model was constructed to describe intramolecular SF occurring in Tc–Ad–Tc (Fig. 7). In this model, ^{1}(^{3}Tc–Ad–^{3}Tc)* and ^{5}(^{3}Tc–Ad–^{3}Tc)* are in a rapid equilibrium. Following its formation by photoexcitation, ^{1}Tc*–Ad–Tc undergoes fluorescence emission, nonradiative deactivation, ISC and SF to form ^{1}(^{3}Tc–Ad–^{3}Tc)*, with rate constants of k_{FL}, k_{NR}, k_{ISC} and k_{SF}, respectively. The sum of k_{FL}, k_{NR} and k_{ISC}, is represented by k_S (Fig. 7). Similarly, ^{1or5}(^{3}Tc–Ad–^{3}Tc)* undergoes TTA, deactivation and dissociation with respective rate constants of k_{TTA}, k_Q and k_{DIS}. Dissociated ^{3}Tc*–Ad–^{3}Tc* undergoes association and deactivation, with respective rate constants of k_{AS} and k_T. The k_S value is replaced by 8.7×10^7 s^{-1}, a

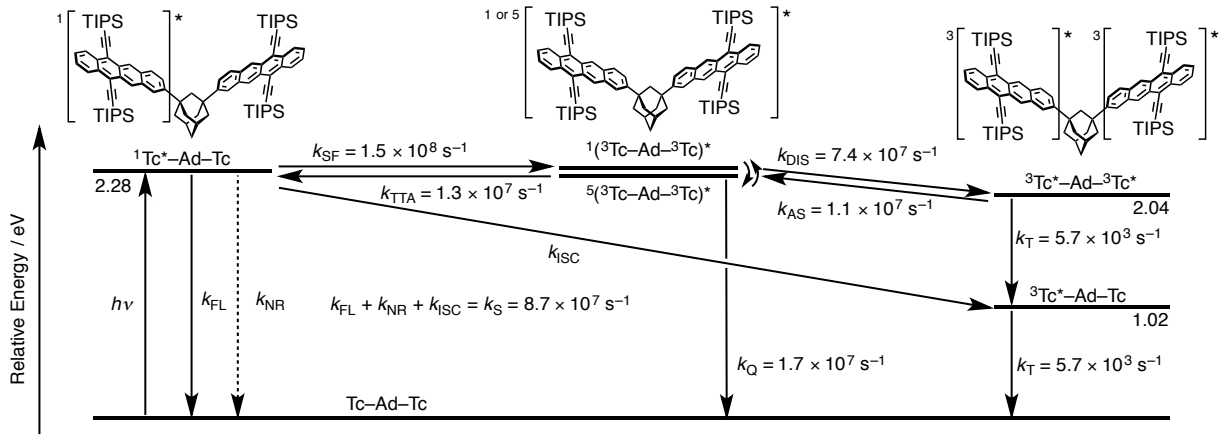

Fig. 7. Energy diagram and kinetic model for intramolecular SF of Tc–Ad–Tc with respective rate constants obtained by using kinetic analysis. ^{1}(^{3}Tc–Ad–^{3}Tc)* and ^{5}(^{3}Tc–Ad–^{3}Tc)* are not distinguished using this analysis, because they are energetically close and interconversion between them is rapid at room temperature.

$$d[^1\text{Tc*–Ad–Tc}]/dt = -(k_S + k_{SF})[^1\text{Tc*–Ad–Tc}] + k_{TTA}[^{1or5}(^3\text{Tc–Ad–}^3\text{Tc})^*] \quad (7)$$

$$d[^{1or5}(^3\text{Tc–Ad–}^3\text{Tc})^*]/dt = k_{SF}[^1\text{Tc*–Ad–Tc}] - (k_{TTA} + k_Q + k_{DIS})[^{1or5}(^3\text{Tc–Ad–}^3\text{Tc})^*] + k_{AS}[^3\text{Tc*–Ad–}^3\text{Tc*}] \quad (8)$$

$$d[^3\text{Tc*–Ad–}^3\text{Tc*}]/dt = k_{DIS}[^{1or5}(^3\text{Tc–Ad–}^3\text{Tc})^*] - (k_{AS} + k_T)[^3\text{Tc*–Ad–}^3\text{Tc*}] \quad (9)$$

value derived from analysis of Tc. The value $k_T = 5.7 \times 10^3$ s^{-1} is the reciprocal of the lifetime (τ_2 in Fig. 6c) of the slowest component of the transient decay profile. When taken together, these relationships lead to the simultaneous differential equations displayed in eqs 7–9. The solution of the these equations, in the form of rate constants given in Fig. 7, are obtained by using the results of arising from analysis of the fluorescence decay profile (Table 1).[59,46] Time-dependent population of the excited species are displayed in Fig. 8. The sum of signals of triplet excitons well reproduced transient absorption trace at 515 nm, where signal of singlet species is negligible.

This analysis strongly demonstrates that the magnitude of k_{SF} of ^{1}Tc*–Ad–Tc is not as large as those of other pentacene dyad systems.[23,24,29] However, the quantum yield of SF ($\Phi_{SF} = k_{SF}/(k_{SF} + k_S)$ = 63%) in this system is larger than those for SF in other tetracene-based systems. The high efficiency probably results from a small k_{TTA} and large k_{DIS}, which are a consequence of weakening of electronic coupling between ^{3}Tc* moieties by the nonconjugated Ad linkage. The Ad linkage brings about weak electronic coupling that enables export of triplet excitons generated by SF via intermolecular energy transfer (eq 10).

$$^3\text{Tc*–Ad–}^3\text{Tc*} + \text{Tc–Ad–Tc} \rightarrow 2\ ^3\text{Tc*–Ad–Tc} \quad (10)$$

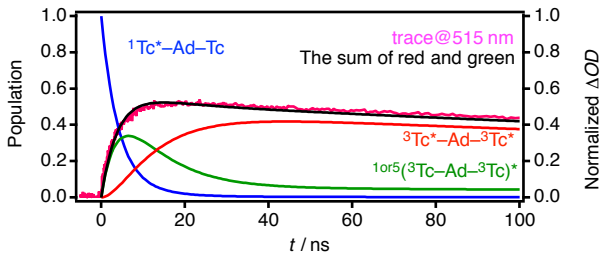

Fig. 8. Time-dependent population of ^{1}Tc*–Ad–Tc (blue), ^{1or5}(^{3}Tc–Ad–^{3}Tc)* (green), and ^{3}Tc*–Ad–^{3}Tc* (red), obtained by kinetic analysis. The sum of triplet species (black) and time-dependent change of transient absorption at 515 nm (pink) were also added.

As described above, the distance and orientation of the Tc moieties are crucial factors in determining the efficiency of SF. The observation that a "flexible C_3-linkage strengthens interactions between π-systems to form intramolecular excimer", is widely known as the Hirayama n = 3 rule.[60] Ad in Tc–Ad–Tc behaves like a C_3-linkage, but being rigid it avoids undesirable formation of intramolecular excimer between the Tc moieties. However, the small spin density at C2 of Ad in ^{5}(^{3}Tc–Ad–^{3}Tc)* (Fig. 9) indicates that interactions between the σ-orbitals of the Ad spacer and π-orbitals of Tc are possible in conformations that enable σ–π overlap. The existence of these types of conformers is well supported by the quintet geometries (anti and syn-conformers, Fig. 5b) characterized by using EPR line-shape analyses. Thus, mixing of σ (and σ*) and π (and π*, respectively) may play a crucial role in governing the efficiency of intramolecular SF and subsequent quintet generation by *J*-modulation. Consequently, substituting the C_3-linkage by an Ad linker in dyads is an effective strategy for promoting rapid intramolecular SF to afford long-lived excitons.

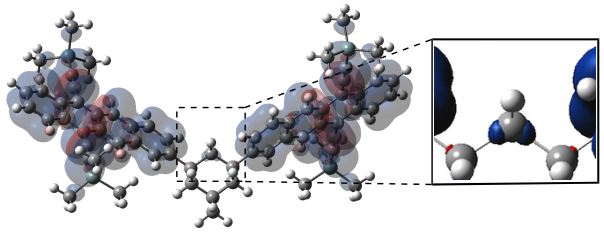

Fig. 9. Spin density distribution of anti-conformation of ^{5}(^{3}Tc'–Ad–^{3}Tc')* and its enlarged view, obtained by B3LYP/6-31G(d).

CONCLUSIONS

The observations made in the investigation described above show that the Ad-linked tetracene dyad Tc–Ad–Tc undergoes exergonic intramolecular SF, while its analog PTc–Ad–PTc does not. The combined results demonstrate that the distance and relative orientation of the Tc moieties in the dyad play crucial roles in promoting intramolecular SF. By employing time-resolved EPR spectroscopy, we characterized geometries of the two distinguishable conformers in the quintet correlated triplet pairs $^5(^3Tc–Ad–^3Tc)^*$. Formation of the long-lived triplet species is caused by weak electronic coupling between Tc moieties occurring through Ad-linker-mediated moderate σ–π interaction. Modulation of σ–π coupling, which enables incoherent singlet–quintet conversions, is governed by molecular motions of the Tc moieties and results in the formation of long-lived quintets that causes separations of the triplet species. Incorporation of rigid aliphatic linkages in dyads provides a way to control the 3D-orientations of π-conjugated systems while leaving the intrinsic S_1 and T_1 levels of the original monomers so that exergonic intramolecular SF can take place and undesirable TTA can be prevented. Long-lived (175 μs) and high-energy (1.03 eV × 2) triplet excitons serve as a promising driving force for charge separation in organic photovoltaics and luminescence organic light-emitting diodes.

ASSOCIATED CONTENT

Supporting Information

The Supporting Information is available free of charge on the Publications website at DOI: XXXX.

Experimental Details, Results of DFT Calculations, Steady State Absorption Spectra of Tc–Ad–Tc in the Frozen Solution, Analysis of Time-resolved EPR Spectra, Analysis of Transient Absorption Spectra of Tc, Tc–Ad–Tc, PTc, and PTc–Ad–PTc, Mathematical Analysis of Time-profiles of Fluorescence Decay, and NMR Spectra.

AUTHOR INFORMATION

Corresponding Author

E-mail: ykobori@kitty.kobe-u.ac.jp (YK)
ikeda@chem.osakafu-u.ac.jp (HI)

ORCID

Yasunori Matsui: 0000-0002-7719-0071

Hiroki Nagashima: 0000-0003-1162-6669

Naoki Okamura: 0000-0002-7180-1863

Takuya Ogaki: 0000-0003-2639-141X

Seiji Akimoto: 0000-0002-8951-8978

Shigeyuki Yagi: 0000-0002-4383-748X

Yasuhiro Kobori: 0000-0001-8370-9362

Hiroshi Ikeda: 0000-0002-8161-2177

Notes

The authors declare no competing financial interests.

Author Contribution

YM, SK, and HN contributed equally.

Present Address

Takuya Ogaki: RIKEN, Center for Emergent Matter Science (CEMS), 2-1 Hirosawa, Wako, Saitama 351-0198, Japan.

ACKNOWLEDGEMENT

This work was partially supported by JSPS KAKENHI Grant (Nos. JP24109009, JP23350023, JP18H01967, JP18K14202, JP17H01265, JP17K19105, JP16H04097). YM was also supported by the Program to Disseminate Tenure Tracking System, MEXT, Japan and Sasakawa Scientific Research Grant from the Japan Science Society (29-303), and joint research program of Molecular Photoscience Research Center, Kobe University. TN was supported by SENTAN, JST.

Dedication

This paper is dedicated to the memory of Prof. Keiji Okada (Osaka City University) and Prof. Kimio Akiyama (Tohoku University).

REFERENCES and NOTES

(1) Smith, M. B.; Michl, J. Singlet Fission. *Chem. Rev.* **2010**, *110* (11), 6891–6936. https://doi.org/10.1021/cr1002613.

(2) Zimmerman, P. M.; Bell, F.; Casanova, D.; Head-Gordon, M. Mechanism for Singlet Fission in Pentacene and Tetracene: From Single Exciton to Two Triplets. *J. Am. Chem. Soc.* **2011**, *133* (49), 19944–19952. https://doi.org/10.1021/ja208431r.

(3) Ito, S.; Nagami, T.; Nakano, M. Molecular Design for Efficient Singlet Fission. *J. Photochem. Photobiol. C Photochem. Rev.* **2018**, *34*, 85–120. https://doi.org/10.1016/j.jphotochemrev.2018.01.002.

(4) Shockley, W.; Queisser, H. J. Detailed Balance Limit of Efficiency of P-n Junction Solar Cells. *J. Appl. Phys.* **1961**, *32* (3), 510–519. https://doi.org/10.1063/1.1736034.

(5) Kim, H.; Keller, B.; Ho-Wu, R.; Abeyasinghe, N.; Vázquez, R. J.; Goodson, T.; Zimmerman, P. M. Enacting Two-Electron Transfer from a Double-Triplet State of Intramolecular Singlet Fission. *J. Am. Chem. Soc.* **2018**, *140* (25), 7760–7763. https://doi.org/10.1021/jacs.8b01884.

(6) Nagata, R.; Nakanotani, H.; Potscavage, W. J.; Adachi, C. Exploiting Singlet Fission in Organic Light-Emitting Diodes. *Adv. Mater.* **2018**, *30* (33), 1801484. https://doi.org/10.1002/adma.201801484.

(7) Allison, R. R.; Sheng, C.; Cuenca, R.; Bagnato, V. S.; Austerlitz, C.; Sibata, C. H. Photodynamic Therapy for Anal Cancer. *Photodiagnosis Photodyn. Ther.* **2010**, *7* (2), 115–119. https://doi.org/10.1016/j.pdpdt.2010.04.002.

(8) DeRosa, M. C.; Crutchley, R. J. Photosensitized Singlet Oxygen and Its Applications. *Coord. Chem. Rev.* **2002**, *233–234*, 351–371. https://doi.org/10.1016/S0010-8545(02)00034-6.

(9) Dillon, R. J.; Piland, G. B.; Bardeen, C. J. Different Rates of Singlet Fission in Monoclinic versus Orthorhombic Crystal

Forms of Diphenylhexatriene. *J. Am. Chem. Soc.* **2013**, *135* (46), 17278–17281. https://doi.org/10.1021/ja409266s.

(10) Weiss, L. R.; Bayliss, S. L.; Kraffert, F.; Thorley, K. J.; Anthony, J. E.; Bittl, R.; Friend, R. H.; Rao, A.; Greenham, N. C.; Behrends, J. Strongly Exchange-Coupled Triplet Pairs in an Organic Semiconductor. *Nat. Phys.* **2017**, *13* (2), 176–181. https://doi.org/10.1038/nphys3908.

(11) Zhu, T.; Wan, Y.; Guo, Z.; Johnson, J.; Huang, L. Two Birds with One Stone: Tailoring Singlet Fission for Both Triplet Yield and Exciton Diffusion Length. *Adv. Mater.* **2016**, *28* (34), 7539–7547. https://doi.org/10.1002/adma.201600968.

(12) Nagashima, H.; Kawaoka, S.; Akimoto, S.; Tachikawa, T.; Matsui, Y.; Ikeda, H.; Kobori, Y. Singlet-Fission-Born Quintet State: Sublevel Selections and Trapping by Multiexciton Thermodynamics. *J. Phys. Chem. Lett.* **2018**, *9* (19), 5855–5861. https://doi.org/10.1021/acs.jpclett.8b02396.

(13) Miyata, K.; Conrad-Burton, F. S.; Geyer, F. L.; Zhu, X. Y. Triplet Pair States in Singlet Fission. *Chem. Rev.* **2019**, acs.chemrev.8b00572. https://doi.org/10.1021/acs.chemrev.8b00572.

(14) Lukman, S.; Musser, A. J.; Chen, K.; Athanasopoulos, S.; Yong, C. K.; Zeng, Z.; Ye, Q.; Chi, C.; Hodgkiss, J. M.; Wu, J.; et al. Tuneable Singlet Exciton Fission and Triplet-Triplet Annihilation in an Orthogonal Pentacene Dimer. *Adv. Funct. Mater.* **2015**, *25* (34), 5452–5461. https://doi.org/10.1002/adfm.201501537.

(15) Sakuma, T.; Sakai, H.; Araki, Y.; Mori, T.; Wada, T.; Tkachenko, N. V.; Hasobe, T. Long-Lived Triplet Excited States of Bent-Shaped Pentacene Dimers by Intramolecular Singlet Fission. *J. Phys. Chem. A* **2016**, *120* (11), 1867–1875. https://doi.org/10.1021/acs.jpca.6b00988.

(16) Liu, H.; Wang, R.; Shen, L.; Xu, Y.; Xiao, M.; Zhang, C.; Li, X. A Covalently Linked Tetracene Trimer: Synthesis and Singlet Exciton Fission Property. *Org. Lett.* **2017**, *19* (3), 580–583. https://doi.org/10.1021/acs.orglett.6b03739.

(17) Korovina, N. V.; Joy, J.; Feng, X.; Feltenberger, C.; Krylov, A. I.; Bradforth, S. E.; Thompson, M. E. Linker-Dependent Singlet Fission in Tetracene Dimers. *J. Am. Chem. Soc.* **2018**, *140* (32), 10179–10190. https://doi.org/10.1021/jacs.8b04401.

(18) Liu, H.; Wang, Z.; Wang, X.; Shen, L.; Zhang, C.; Xiao, M.; Li, X. Singlet Exciton Fission in a Linear Tetracene Tetramer. *J. Mater. Chem. C* **2018**, *6* (13), 3245–3253. https://doi.org/10.1039/c7tc05783k.

(19) Müller, A. M.; Avlasevich, Y. S.; Müllen, K.; Bardeen, C. J. Evidence for Exciton Fission and Fusion in a Covalently Linked Tetracene Dimer. *Chem. Phys. Lett.* **2006**, *421* (4–6), 518–522. https://doi.org/10.1016/j.cplett.2006.01.117.

(20) Sanders, S. N.; Kumarasamy, E.; Pun, A. B.; Trinh, M. T.; Choi, B.; Xia, J.; Taffet, E. J.; Low, J. Z.; Miller, J. R.; Roy, X.; et al. Quantitative Intramolecular Singlet Fission in Bipentacenes. *J. Am. Chem. Soc.* **2015**, *137* (28), 8965–8972. https://doi.org/10.1021/jacs.5b04986.

(21) Chen, M.; Krzyaniak, M. D.; Nelson, J. N.; Bae, Y. J.; Harvey, S. M.; Schaller, R. D.; Young, R. M.; Wasielewski, M. R. Quintet-Triplet Mixing Determines the Fate of the Multiexciton State Produced by Singlet Fission in a Terrylenediimide Dimer at Room Temperature. *Proc. Natl. Acad. Sci.* **2019**, 201820932. https://doi.org/10.1073/pnas.1820932116.

(22) Hetzer, C.; Guldi, D. M.; Tykwinski, R. R. Pentacene Dimers as a Critical Tool for the Investigation of Intramolecular Singlet Fission. *Chem. Eur. J.* **2018**, *24* (33), 8245–8257. https://doi.org/10.1002/chem.201705355.

(23) Basel, B. S.; Zirzlmeier, J.; Hetzer, C.; Phelan, B. T.; Krzyaniak, M. D.; Reddy, S. R.; Coto, P. B.; Horwitz, N. E.; Young, R. M.; White, F. J.; et al. Unified Model for Singlet Fission within a Non-Conjugated Covalent Pentacene Dimer. *Nat. Commun.* **2017**, *8*, 15171. https://doi.org/10.1038/ncomms15171.

(24) Pun, A. B.; McCamey, D. R.; Kumarasamy, E.; Paley, D. W.; Fuemmeler, E. G.; Choi, B.; Yablon, L. M.; Asadpoordarvish, A.; Steigerwald, M. L.; Sfeir, M. Y.; et al. Tuning Singlet Fission in π-Bridge-π Chromophores. *J. Am. Chem. Soc.* **2017**, *139* (36), 12488–12494. https://doi.org/10.1021/jacs.7b05204.

(25) Cook, J. D.; Carey, T. J.; Damrauer, N. H. Solution-Phase Singlet Fission in a Structurally Well-Defined Norbornyl-Bridged Tetracene Dimer. *J. Phys. Chem. A* **2016**, *120* (26), 4473–4481. https://doi.org/10.1021/acs.jpca.6b04367.

(26) Damrauer, N. H.; Snyder, J. L. Symmetry-Directed Control of Electronic Coupling for Singlet Fission in Covalent Bis-Acene Dimers. *J. Phys. Chem. Lett.* **2015**, *6* (22), 4456–4462. https://doi.org/10.1021/acs.jpclett.5b02186.

(27) Basel, B. S.; Zirzlmeier, J.; Hetzer, C.; Reddy, S. R.; Phelan, B. T.; Krzyaniak, M. D.; Volland, M. K.; Coto, P. B.; Young, R. M.; Clark, T.; et al. Evidence for Charge-Transfer Mediation in the Primary Events of Singlet Fission in a Weakly Coupled Pentacene Dimer. *Chem* **2018**, *4* (5), 1092–1111. https://doi.org/10.1016/j.chempr.2018.04.006.

(28) Cook, J. D.; Carey, T. J.; Arias, D. H.; Johnson, J. C.; Damrauer, N. H. Solvent-Controlled Branching of Localized versus Delocalized Singlet Exciton States and Equilibration with Charge Transfer in a Structurally Well-Defined Tetracene Dimer. *J. Phys. Chem. A* **2017**, *121* (48), 9229–9242. https://doi.org/10.1021/acs.jpca.7b09458.

(29) Zirzlmeier, J.; Lehnherr, D.; Coto, P. B.; Chernick, E. T.; Casillas, R.; Basel, B. S.; Thoss, M.; Tykwinski, R. R.; Guldi, D. M. Singlet Fission in Pentacene Dimers. *Proc. Natl. Acad. Sci.* **2015**, *112* (17), 5325–5330. https://doi.org/10.1073/pnas.1422436112.

(30) Nakamura, S.; Sakai, H.; Nagashima, H.; Kobori, Y.; Tkachenko, N. V; Hasobe, T. Quantitative Sequential Photoenergy Conversion Process from Singlet Fission to Intermolecular Two-Electron Transfers Utilizing Tetracene Dimer. *ACS Energy Lett.* **2019**, *4* (1), 26–31. https://doi.org/10.1021/acsenergylett.8b01964.

(31) Yamakado, T.; Takahashi, S.; Watanabe, K.; Matsumoto, Y.; Osuka, A.; Saito, S. Conformational Planarization versus Singlet Fission: Distinct Excited-State Dynamics of Cyclooctatetraene-Fused Acene Dimers. *Angew. Chem. Int. Ed.* **2018**, *57* (19), 5438–5443. https://doi.org/10.1002/anie.201802185.

(32) Sanders, S. N.; Kumarasamy, E.; Pun, A. B.; Steigerwald, M. L.; Sfeir, M. Y.; Campos, L. M. Intramolecular Singlet Fission in Oligoacene Heterodimers. *Angew. Chem. Int. Ed.* **2016**, *55*

(10), 3373–3377. https://doi.org/10.1002/anie.201510632.

(33) Nakagawa, T.; Okamoto, K.; Hanada, H.; Katoh, R. Probing with Randomly Interleaved Pulse Train Bridges the Gap between Ultrafast Pump-Probe and Nanosecond Flash Photolysis. *Opt. Lett.* **2016**, *41* (7), 1498. https://doi.org/10.1364/ol.41.001498.

(34) Aratani, Y.; Oyama, K.; Suenobu, T.; Yamada, Y.; Fukuzumi, S. Photocatalytic Hydroxylation of Benzene by Dioxygen to Phenol with a Cyano-Bridged Complex Containing FeII and RuII Incorporated in Mesoporous Silica-Alumina. *Inorg. Chem.* **2016**, *55* (12), 5780–5786. https://doi.org/10.1021/acs.inorgchem.5b02909.

(35) Aratani, Y.; Suenobu, T.; Ohkubo, K.; Yamada, Y.; Fukuzumi, S. Dual Function Photocatalysis of Cyano-Bridged Heteronuclear Metal Complexes for Water Oxidation and Two-Electron Reduction of Dioxygen to Produce Hydrogen Peroxide as a Solar Fuel. *Chem. Commun.* **2017**, *53* (24), 3473–3476. https://doi.org/10.1039/C7CC00621G.

(36) Ota, W.; Matsunaga, H.; Teranishi, T.; Lian, Z.; Kurata, H.; Haruta, M.; Yamakata, A.; Sakamoto, M.; Sato, T.; Vequizo, J. J. M. Near Infrared Light Induced Plasmonic Hot Hole Transfer at a Nano-Heterointerface. *Nat. Commun.* **2018**, *9* (1), 2314. https://doi.org/10.1038/s41467-018-04630-w.

(37) Tsudaka, T.; Kotani, H.; Ohkubo, K.; Nakagawa, T.; Tkachenko, N. V.; Lemmetyinen, H.; Fukuzumi, S. Photoinduced Electron Transfer in 9-Substituted 10-Methylacridinium Ions. *Chem. Eur. J.* **2017**, *23* (6), 1306–1317. https://doi.org/10.1002/chem.201604527.

(38) Stokkum, I. H. M. van; Mullen, K. M.; Seger, R.; Snellenburg, J. J.; Laptenok, S. P. Glotaran : A Java -Based Graphical User Interface for the R Package TIMP . *J. Stat. Softw.* **2015**, *49*(3), 1–23. https://doi.org/10.18637/jss.v049.i03.

(39) Hasegawa, M.; Nagashima, H.; Minobe, R.; Tachikawa, T.; Mino, H.; Kobori, Y. Regulated Electron Tunneling of Photoinduced Primary Charge-Separated State in the Photosystem II Reaction Center. *J. Phys. Chem. Lett.* **2017**, *8* (6), 1179–1184. https://doi.org/10.1021/acs.jpclett.7b00044.

(40) Frisch, M. J.; Trucks, G. W.; Schlegel, H. B.; Scuseria, G. E.; Robb, M. A.; Cheeseman, J. R.; Scalmani, G.; Barone, V.; Mennucci, B.; Petersson, G. A.; et al. *Gaussian 09*; 2009.

(41) Hanwell, M. D.; Curtis, D. E.; Lonie, D. C.; Vandermeerschd, T.; Zurek, E.; Hutchison, G. R. Avogadro: An Advanced Semantic Chemical Editor, Visualization, and Analysis Platform. *J. Cheminform.* **2012**, *4* (8), 17. https://doi.org/10.1186/1758-2946-4-17.

(42) Dennington, R.; Keith, T.; Millam, J. Gaussview, Version 5. *Semichem Inc. , Shawnee Mission, KS*. 2016, p Semichem Inc.

(43) Sato, R.; Kitoh-Nishioka, H.; Kamada, K.; Mizokuro, T.; Kobayashi, K.; Shigeta, Y. Does Inactive Alkyl Chain Enhance Triplet-Triplet Annihilation of 9,10-Diphenylanthracene Derivatives? *J. Phys. Chem. C* **2018**, *122* (10), 5334–5340. https://doi.org/10.1021/acs.jpcc.8b01328.

(44) Zang, H.; Zhao, Y.; Liang, W. Quantum Interference in Singlet Fission: J- and H-Aggregate Behavior. *J. Phys. Chem. Lett.* **2017**, *8* (20), 5105–5112. https://doi.org/10.1021/acs.jpclett.7b01996.

(45) Anthony, J.; Friend, R. H.; Parkinson, P.; Walker, B. J.; Herz, L. M.; Gelinas, S.; Musser, A. J.; Bruzek, M. J.; Stern, H. L. Identification of a Triplet Pair Intermediate in Singlet Exciton Fission in Solution. *Proc. Natl. Acad. Sci.* **2015**, *112* (25), 7656–7661. https://doi.org/10.1073/pnas.1503471112.

(46) For the detail, See the Supporting Information.

(47) Uoyama, H.; Goushi, K.; Shizu, K.; Nomura, H.; Adachi, C. Highly Efficient Organic Light-Emitting Diodes from Delayed Fluorescence. *Nature* **2012**, *492* (7428), 234–238. https://doi.org/10.1038/nature11687.

(48) Kim, G. H.; Lampande, R.; Im, J. B.; Lee, J. M.; Lee, J. Y.; Kwon, J. H. Controlling the Exciton Lifetime of Blue Thermally Activated Delayed Fluorescence Emitters Using a Heteroatom-Containing Pyridoindole Donor Moiety. *Mater. Horizons* **2017**, *4* (4), 619–624. https://doi.org/10.1039/c6mh00579a.

(49) Kaji, H.; Suzuki, H.; Fukushima, T.; Shizu, K.; Suzuki, K.; Kubo, S.; Komino, T.; Oiwa, H.; Suzuki, F.; Wakamiya, A.; et al. Purely Organic Electroluminescent Material Realizing 100% Conversion from Electricity to Light. *Nat. Commun.* **2015**, *6* (1), 1–8. https://doi.org/10.1038/ncomms9476.

(50) Stoll, S.; Schweiger, A. EasySpin, a Comprehensive Software Package for Spectral Simulation and Analysis in EPR. *J. Magn. Reson.* **2006**, *178* (1), 42–55. https://doi.org/10.1016/j.jmr.2005.08.013.

(51) Benk, H.; Sixl, H. Theory of Two Coupled Triplet States. *Mol. Phys.* **2006**, *42* (4), 779–801. https://doi.org/10.1080/00268978100100631.

(52) Lubert-Perquel, D.; Salvadori, E.; Dyson, M.; Stavrinou, P. N.; Montis, R.; Nagashima, H.; Kobori, Y.; Heutz, S.; Kay, C. W. M. Identifying Triplet Pathways in Dilute Pentacene Films. *Nat. Commun.* **2018**, *9* (1), 4222. https://doi.org/10.1038/s41467-018-06330-x.

(53) Tayebjee, M. J. Y.; Sanders, S. N.; Kumarasamy, E.; Campos, L. M.; Sfeir, M. Y.; McCamey, D. R. Quintet Multiexciton Dynamics in Singlet Fission. *Nat. Phys.* **2017**, *13* (2), 182–188. https://doi.org/10.1038/nphys3909.

(54) Yamauchi, S.; Takahashi, A.; Iwasaki, Y.; Unno, M.; Ohba, Y.; Higuchi, J.; Blank, A.; Levanon, H. The Lowest Photoexcited Triplet State of Subphthalocyanine in Solid and Fluid Environments. Time-Resolved Electron Paramagnetic Resonance Studies. *J. Phys. Chem. A* **2003**, *107* (10), 1478–1485. https://doi.org/10.1021/jp0258210.

(55) Tan, R.-R.; Shen, X.; Hu, L.; Zhang, F.-S. Liquid-to-Glass Transition of Tetrahydrofuran and 2-Methyltetrahydrofuran. *Chinese Phys. B* **2012**, *21* (8), 086402. https://doi.org/10.1088/1674-1056/21/8/086402.

(56) Brown, I. M. Electron Spin-Echo Envelope Decays and Molecular Motion: Rotational and Translational Diffusion. *J. Chem. Phys.* **1974**, *60* (12), 4930–4938. https://doi.org/10.1063/1.1681005.

(57) Kobori, Y.; Shibano, Y.; Endo, T.; Tsuji, H.; Murai, H.; Tamao, K. Time-Resolved EPR Characterization of a Folded Conformation of Photoinduced Charge-Separated State in Porphyrin Fullerene Dyad Bridged by Diphenyldisilane. *J.*

Am. Chem. Soc. **2009**, *131* (5), 1624–1625. https://doi.org/10.1021/ja8073775.

(58) Shushin, A. I. The Relaxational Mechanism of Net CIDEP Generation in Triplet-Radical Quenching. *Chem. Phys. Lett.* **1993**, *208* (3–4), 173–178. https://doi.org/10.1016/0009-2614(93)89057-O.

(59) *Mathematica 11.1.1*; Wolfram Research, Inc.: Champaign, IL, 2017.

(60) Hirayama, F. Intramolecular Excimer Formation. I. Diphenyl and Triphenyl Alkanes. *J. Chem. Phys.* **1965**, *42* (9), 3163–3171. https://doi.org/10.1063/1.1696395.

Graphical Abstract